Langmuir

Article

pubs.acs.org/Langmuir

Amyloid β Peptide Conformational Changes in the Presence of a Lipid Membrane System

Angelo Accardo,*[,†] Victoria Shalabaeva,[†] Marine Cotte,[‡,§] Manfred Burghammer,[‡,⊥] Roman Krahne,[†] Christian Riekel,[‡] and Silvia Dante*[,∥]

[†]Nanostructures Department, Istituto Italiano di Tecnologia, Via Morego 30, Genova 16163, Italy

[‡]European Synchrotron Radiation Facility, CS 40220, F-38043 Grenoble Cedex 9, France

[§]Laboratoire d'Archéologie Moléculaire et Structurale, LAMS, UMR 8220, CNRS F-75005, Paris, France

[⊥]Department of Analytical Chemistry, Ghent University, Krijgslaan 281, S12, B-9000 Ghent, Belgium

[∥]Nanophysics Department, Istituto Italiano di Tecnologia, Via Morego 30, Genova 16163, Italy

Supporting Information

ABSTRACT: Here we are presenting a comparative analysis of conformational changes of two amyloid β peptides, Aβ(25−35) and Aβ(1−42), in the presence and absence of a phospholipid system, namely, POPC/POPS (1-palmitoyl-2-oleoylphospatidylcholine/palmitoyl-2-oleoylphospatidylserine), through Raman spectroscopy, synchrotron radiation micro Fourier-transform infrared spectroscopy, and micro X-ray diffraction. Ringlike samples were obtained from the evaporation of pure and mixed solutions of the proteins together with the POPC/POPS system on highly hydrophilic substrates. The results confirm the presence of a α-helical to β-sheet transition from the internal rim of the ringlike samples to the external one in the pure Aβ(25−35) residual, probably due to the convective flow inside the droplets sitting on highly hydrophilic substrates enhancing the local concentration of the peptide at the external edge of the dried drop. In contrast, the presence of POPC/POPS lipids in the peptide does not result in α-helical structures and introduces the presence of antiparallel β-sheet material together with parallel β-sheet structures and possible β-turns. As a control, Aβ(1−42) peptide was also tested and shows β-sheet conformations independently from the presence of the lipid system. The μXRD analysis further confirmed these conclusions, showing how the absence of the phospholipid system induces in the Aβ(25−35) a probable composite α/β material while its coexistence with the peptide leads to a not oriented β-sheet conformation. These results open interesting scenarios on the study of conformational changes of Aβ peptides and could help, with further investigations, to better clarify the role of enzymes and alternative lipid systems involved in the amyloidosis process of Aβ fragments.

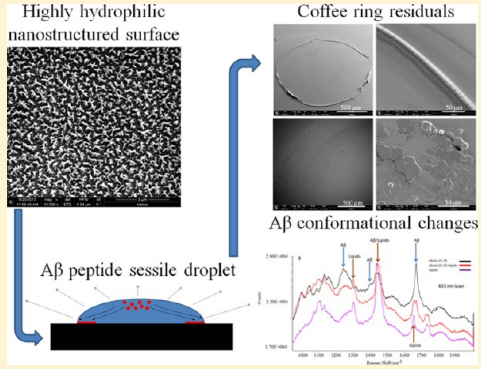

INTRODUCTION

Extracellular amyloid plaques are a hallmark material for the study of Alzheimer disease.[1,2] The neurotoxicity of their main components, the amyloid β peptides (Aβs), may be mediated by direct interaction between the peptides and the neural lipid membrane.[3] The involvement of the neural membrane in fibrillogenesis has also to be clarified in view of the central function assumed by the membrane-bound amyloid precursor protein (APP).[4] Studies on membrane model systems suggest an active role of the lipid membrane in protein misfolding, amyloid formation, and toxicity.[3,5−7] Depending on its chemistry, the membrane surface may locally act as a catalyzer for peptide misfolding, producing toxic intermediates and triggering fibrillogenesis. Different Aβ species or intermediates can also introduce modifications to lipid membranes ranging from disruption[8] to ion permeabilization[9] to mechanical destabilization.[10] Among the different Aβ species, the main component of senile plaques, Aβ(1−42), is considered to be a possible trigger of the neurodegenerative cascade, due to its proven cytotoxicity.[11] Indeed, Aβ(1−42) combined with model lipid systems induces fusion of unilamellar vesicles (ULV)[12] and membrane disruption.[8,10] The shorter Aβ(25−35) species is also membrane active[13] and retains much of the Aβ(1−42) biological and neurotoxic activities.[14]

In order to shed more light on conformational and structural processes of amyloidosis involving membranes, we are exploring the Aβ(25−35) and Aβ(1−42) species by a combination of micro-Raman (μRaman), synchrotron radiation (SR) micro Fourier-transform infrared spectroscopy (μFTIR), and micro X-ray diffraction (μXRD) probes. In order to enhance the sensitivity of these probes, we deposited droplets with Aβ and phospholipid solutes on highly hydrophilic nanostructured substrates. The aggregation mechanism of solute in droplet residues has been extensively exploited for

Received: January 14, 2014
Revised: February 25, 2014
Published: February 27, 2014

   dx.doi.org/10.1021/la500145r | Langmuir 2014, 30, 3191−3198

in situ characterization of biological processes such as crystallization,[15,16] amyloid formation,[17,18] and cellular membrane exosome discrimination.[19] Here we principally focused on the α/β transition of Aβ(25−35) in the presence and absence of a phospholipid mixtures made of POPC (1-palmitoyl-2-oleoylphospatidylcholine) and POPS (1-palmitoyl-2-oleoylphospatidylserine). As in our previous investigations,[12,13] we have chosen a POPC/POPS 9:1 mol/mol mixture to mimic the phospholipid composition of the neural membranes, in terms of alkyl chain unsaturation and negative charge. The results obtained with Aβ(25−35) contrast those of Aβ(1−42), which always show a β-type conformation, independently from the presence of the phospholipid system. The various probes used suggest a possible scenario for the α/β transition pathway of Aβ(25−35) in the absence and presence of the phospholipid system.

EXPERIMENTAL SECTION

Peptides and Lipids. Aβ(1−42) and Aβ(25−35) were purchased from Bachem, while POPC and POPS[10] were from Avanti Polar Lipids (Alabaster, AL). Solvents were obtained from Sigma-Aldrich. POPC and POPS were dissolved at a 9:1 mol/mol ratio in chloroform:methanol 2:1, desiccated under nitrogen flux, and dried under vacuum overnight. Lipids were resuspended in Milli-Q water at a concentration of 5 mg/mL and allowed to swell for 30 min. LUVs (large unilamellar vesicles) were prepared by extrusion through pores of 100 nm in diameter. Aβ(1−42) and Aβ(25−35) were first dissolved in trifluoroacetic acid (TFA) at a concentration 1 mg/mL to eliminate the presence of seeds and to obtain a monomeric peptide dispersion. TFA was dried under nitrogen, and the peptides were successively dissolved in Milli-Q water (1 mg/mL), shortly sonicated, and centrifuged at 1000 rpm for 10 min.

Substrate Preparation. Highly hydrophilic substrates were prepared from commercial CaF_2/BaF_2 windows (Crystran) and Si_3N_4 windows (Silson) by spin-coating liquid PMMA A11 (Microchem) at 2000 rpm for 60 s, baking it (180 °C for 30 min), and finally texturing it by oxygen plasma reactive ion etch[16] (Sentech; parameters: ICP 50 W, RF 100 W, pressure 6.5 Pa, oxygen flow 30 sccm, 5 min).

μRaman, μFTIR, and μXRD Configurations. μRaman experiments were performed in transmission with an In-Via Renishaw microRaman setup using both 532 and 633 nm laser lines with a 50× objective. μFTIR experiments were performed in transmission mode at the ESRF-ID21 beamline with a 6 μm × 6 μm beam and a Mercury Cadmium Telluride (MCT) detector, while microbeam small-angle and wide-angle X-ray scattering experiments (μSAXS/WAXS) were conducted at the ESRF-ID13 beamline.[15] A monochromatic beam of λ = 0.9765 Å was focused to a 1.3 (h) × 1.5 (w) μm^2 spot with about 3 × 10^{11} ph/s flux at the sample position using a transfocator[20] based on parabolic Be-refractive lenses. A Frelon CCD detector with 2048 × 2048 pixels of 50 × 50 μm^2 each (binned to 4 × 4) was used for data collection with an exposure of 0.5 s per pattern. The distance sample-to-detector was calibrated to 124.05 mm by an Ag-behenate calibrant.[21]

Scanning Electron Microscopy (SEM). SEM images were recorded by a FEI HELIOS Nanolab 600 instrument with a 3−5 kV acceleration voltage on samples sputtered with a 10 nm layer of gold.

RESULTS AND DISCUSSION

About 3 μL solution drops of amyloid peptides in the presence and absence of phospholipid vesicles were deposited by a pipet on 1 mm thick CaF_2/BaF_2 highly hydrophilic windows and on 200 nm Si_3N_4 membranes, respectively, for the μRaman/μFTIR experiments and for the μXRD experiments to avoid any interfering signal coming from the supports. Ringlike solid residues were formed almost immediately due to the strong heterogeneous evaporation rate on hydrophilic substrates.

Scanning Electron Microscopy. The SEM micrographs of Aβ(25−35) and Aβ(25−35) + POPC/POPS residuals dried on highly hydrophilic BaF_2 windows show characteristic coffee ring residues (Figure 1). The Aβ(25−35) coffee ring clearly shows

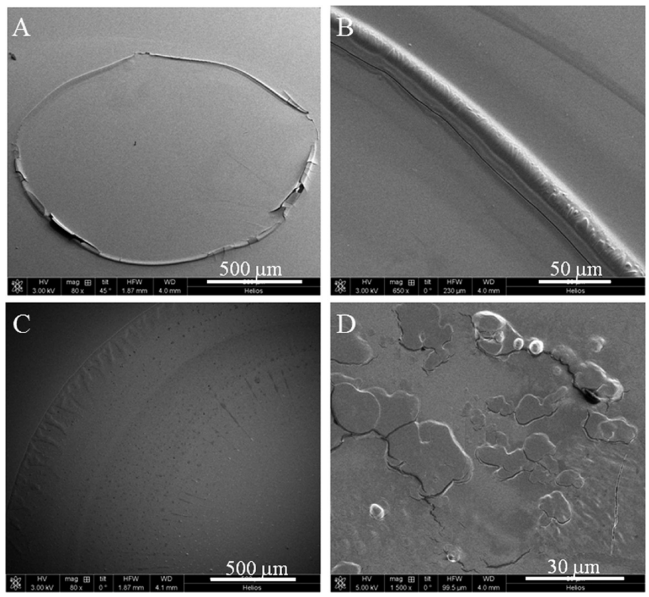

Figure 1. SEM micrographs of Aβ(25−35) (A, B) and Aβ(25−35) + POPC/POPS (C, D) residues.

substructures (Figure 1A,B). The Aβ(25−35) + POPC/POPS shows, however, only a weak coffee-ring effect at the outer rim of the residue (Figure 1C) in addition to lipid patches with integrated peptide material (Figure 1D).

μRaman. Small portions of the external edge of the residual were illuminated at high lateral spatial resolution (<1 μm) in different positions of the whole ring to be sure that the conformation was always the same. The same points were further analyzed by μFTIR and μXRD, as shown in the following sections. Spectra of pure Aβ(25−35) and in presence of POPC/POPS are shown in Figure 2. Conformational information was obtained by analyzing the amide I and amide III bands:[22,23] the 1239 cm^{-1} peak is characteristic of amide III β-conformations, the 1260−1300 cm^{-1} band was attributed to α-helix material and the 1240−1250 cm^{-1} band to unordered material, the 1395 cm^{-1} peak is related to the so-called amide S (whose presence is related to β-sheet material[24]), and the 1668 cm^{-1} peak is linked to amide I β-sheet material. The 1443 cm^{-1} peak was assigned to the CH_2 scissoring mode and the 1732 cm^{-1} peak to the ester carbonyl stretch. These bands overlap in the presence of the POPC/POPS vesicles with characteristic lipid bands,[25] in particular, the 1300 cm^{-1} peak, which for the lipid systems represents the CH_2 twisting mode while for peptides could be related to the α-helix amide III region (1260−1300 cm^{-1}).

The 1653 cm^{-1} peak corresponds for lipids to the *cis*-carbon double bond and for peptides to the α-helix amide I region (1645−1660 cm^{-1}). The merging of these peaks in the mixed system Aβ(25−35) + POPC/POPS, however, did not allow a conclusion with respect to the presence of α-helix material.

μFTIR. Complementary μFTIR allowed addressing the presence of α-helical features. Before the experiment we ensured that the signal coming from the highly hydrophilic substrates was not interfering with the amide I band (Figure S1,

dx.doi.org/10.1021/la500145r | Langmuir 2014, 30, 3191−3198

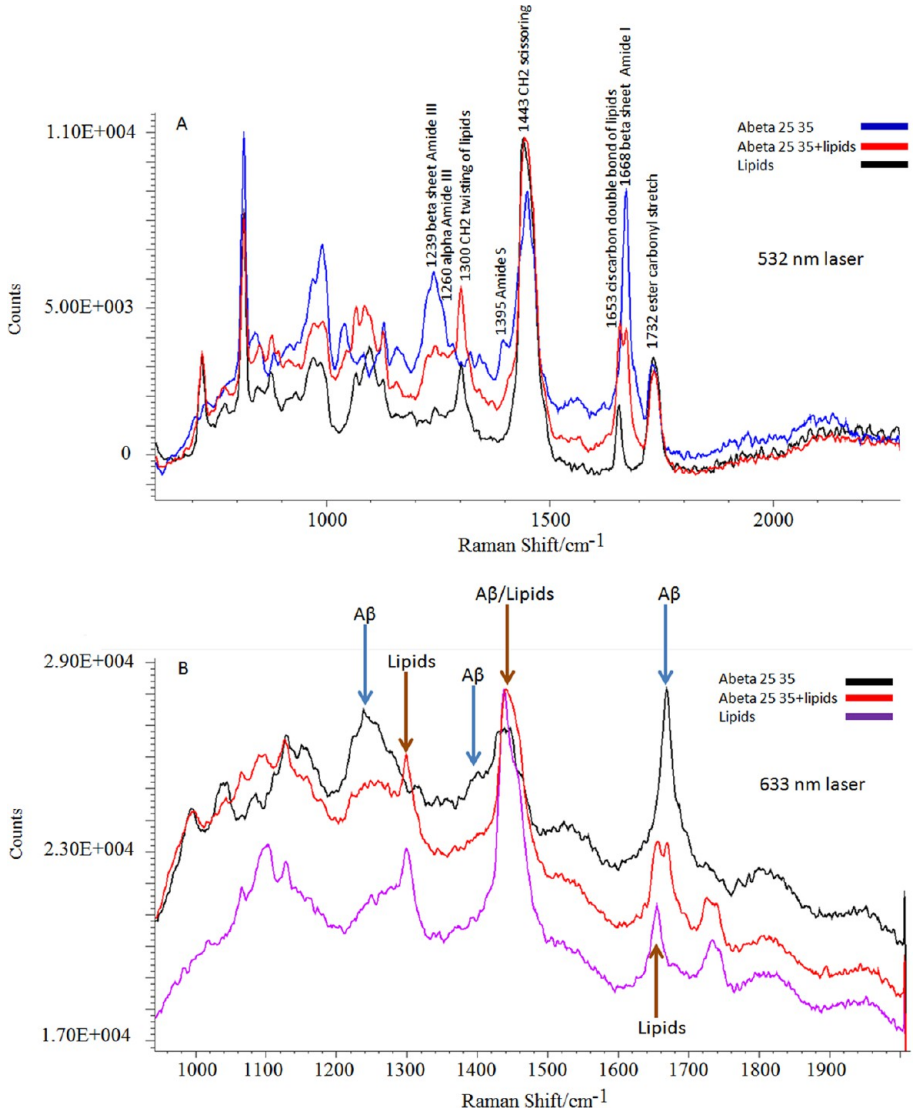

Figure 2. Raman spectra recorded from the coffee stain residues of the Aβ(25−35), lipids, and Aβ(25−35) + lipid systems with excitation wavelength of 532 nm (A) and 633 nm (B) (The arrows indicate the main Aβ and lipid peaks).

Supporting Information). The FTIR spectra of the solid rim regions of pure Aβ(25−35), revealed in the SEM images (Figure 1), are shown in Figure 3. The outer rim (Figure 3A,B) is characterized by parallel β-sheet material (peak at 1634 cm^{-1}), while the inner zone (Figure 3C−E) is characterized by a α-helical material (1657 cm^{-1}).[26] The same conformations were observed in other regions of the coffee-ring residue.

The conformational change from α-helical material at the inner rim to β-sheet material at the outer rim can be explained by a Marangoni-type flow. The high evaporation flux at the triple contact line[27,28] results in an accumulation of solute while the inner regions are depleted (Figure 4). The convective flow and the enhanced peptide concentration in proximity of the external rim have been shown to result in self-assembly of amyloid fibrils.[17] The lower amount of peptide material at the inner rim is not sufficient for the α/β transition and the material remains arrested in a α-helical conformation.

As the μFTIR spectra of the pure lipids did not overlap in the amide I regions of the Aβ peptide [Figures 5 and S2 (Supporting Information)], we were able for the Aβ(25−35)/POPC/POPS mixture to clearly identify the exclusive presence of β-sheet material without any trace of α-helices (Figure 5).

In particular, the analysis showed the presence of antiparallel β-sheets (1685 cm^{-1}) together with parallel β-sheets (1634 cm^{-1}) and possible β-turns (1670 cm^{-1}).[26] The presence of α-helical material was completely excluded by probing the whole sample (Figure S3, Supporting Information), confirming that antiparallel conformations (1685 cm^{-1}) are prominent in the inner part of the sample while the 1634 cm^{-1} band indicated preferentially parallel β-sheet conformations in the outer rim. This is attributed to the presence of the phospholipids that influence the fibrillation process, as demonstrated by previous studies.[29,30]

The β-sheet conformation mentioned above also confirms studies that showed an antiparallel β-sheet organization at early stages of aggregation by the ∼1690 cm^{-1} band, while the parallel β-sheet organization with a band around 1630 cm^{-1} appeared during fibrillation.[31] In summary, we found for pure Aβ(25−35) the presence of α-helical material in the inner rim and β-type material in the outer rim. In contrast, for the Aβ(25−35) + POPC/POPS mixture, the β-material in the

dx.doi.org/10.1021/la500145r | Langmuir 2014, 30, 3191−3198

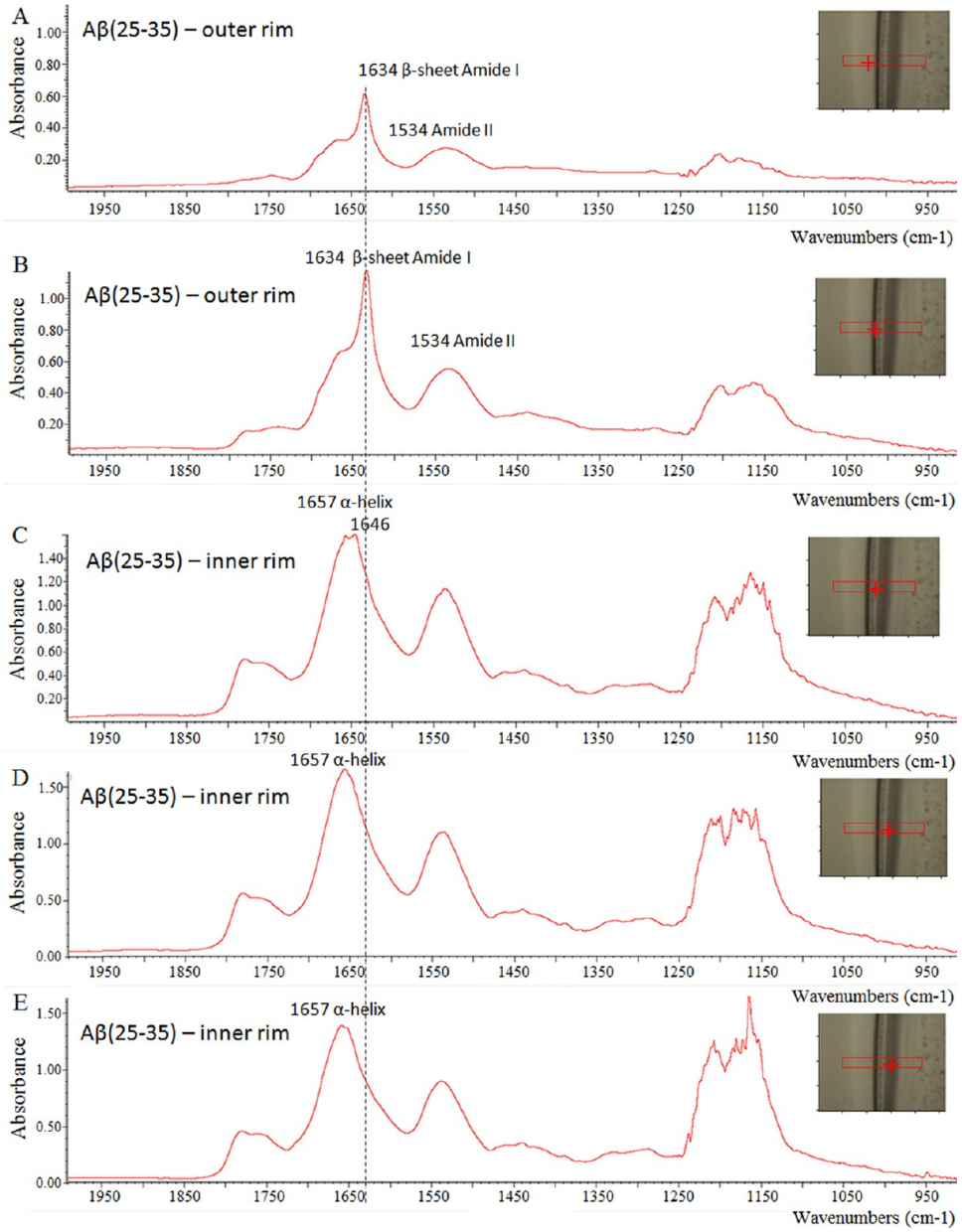

Figure 3. FTIR spectra recorded from several regions of the Aβ(25−35) residue dried on highly hydrophilic BaF_2 surfaces (Insets: optical images of the coffee-ring edge; the red cross represents the position of the beam).

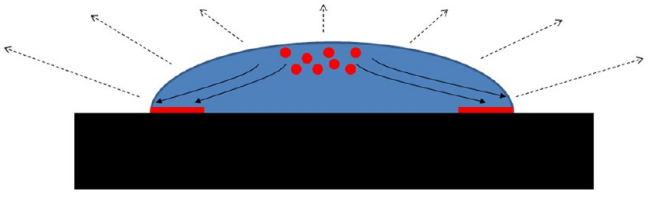

Figure 4. Sketch of an evaporating droplet on a hydrophilic substrate. The evaporation rate is stronger near the contact line, provoking a radial convective motion from the center toward the contact line.

outer rim consists of both β-turns and parallel β-sheet components but of preferentially antiparallel β-sheets in the inner part. With respect to the lipids [Figure 5 and S2 (Supporting Information)], we could clearly recognize the 1739 cm^{-1} peak of the C═O stretch of esters, the 1465 cm^{-1} peak of C−H deformation of CH_2, the spectral band at 1220−1250 cm^{-1} related to phosphodiesters, and the 900−1200 cm^{-1} band related to carbohydrates.[26] We note that the phosphodiester peak strongly decreased in the presence of Aβ (25−35), indicating a possible direct interaction of the peptide with the lipid head groups. μFTIR experiments on Aβ(1−42) in the presence and absence of the POPC/POPS following the same protocol revealed in both cases the presence of parallel β-sheet material (1631 cm^{-1} peak; Figure S4, Supporting Information).

μXRD. Complementary information on the crystalline fractions of the lipid and peptide system was obtained by micro small and wide angle X-ray scattering (μSAXS/WAXS). Inspection of a raster-scan of the rim of the pure lipid solution residue reveals no apparent local structural variations. A detailed analysis of a selected pattern suggests, however, the presence of several phospholipid phases. Indeed, we observe a broad powder ring (d = 4.6 Å) overlapping a narrow 4.2 Å peak with a narrow azimuthal profile (Figures 6A,C,D). We attribute

dx.doi.org/10.1021/la500145r | *Langmuir* 2014, 30, 3191−3198

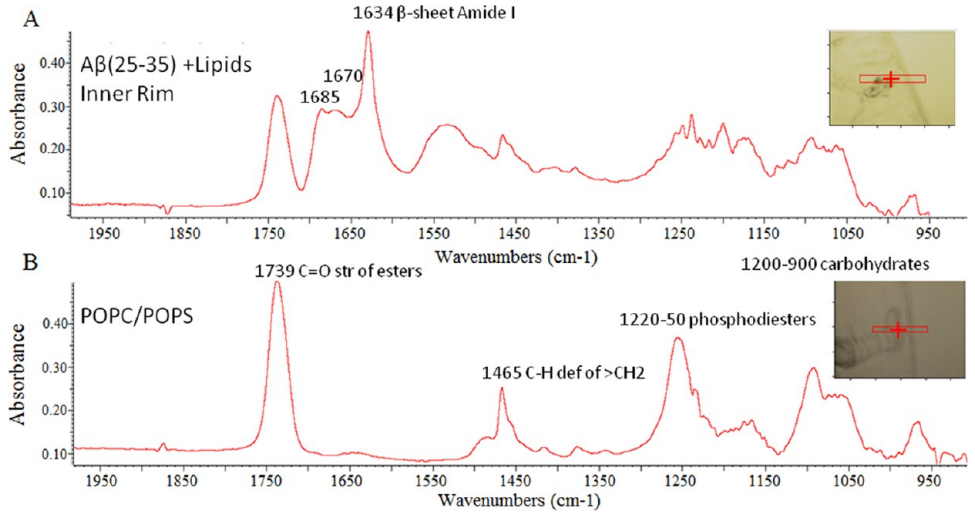

Figure 5. FTIR spectra of the Aβ(25−35) + POPC/POPS (A) and pure POPC/POPS (B) residues dried on highly hydrophilic BaF_2 surfaces.

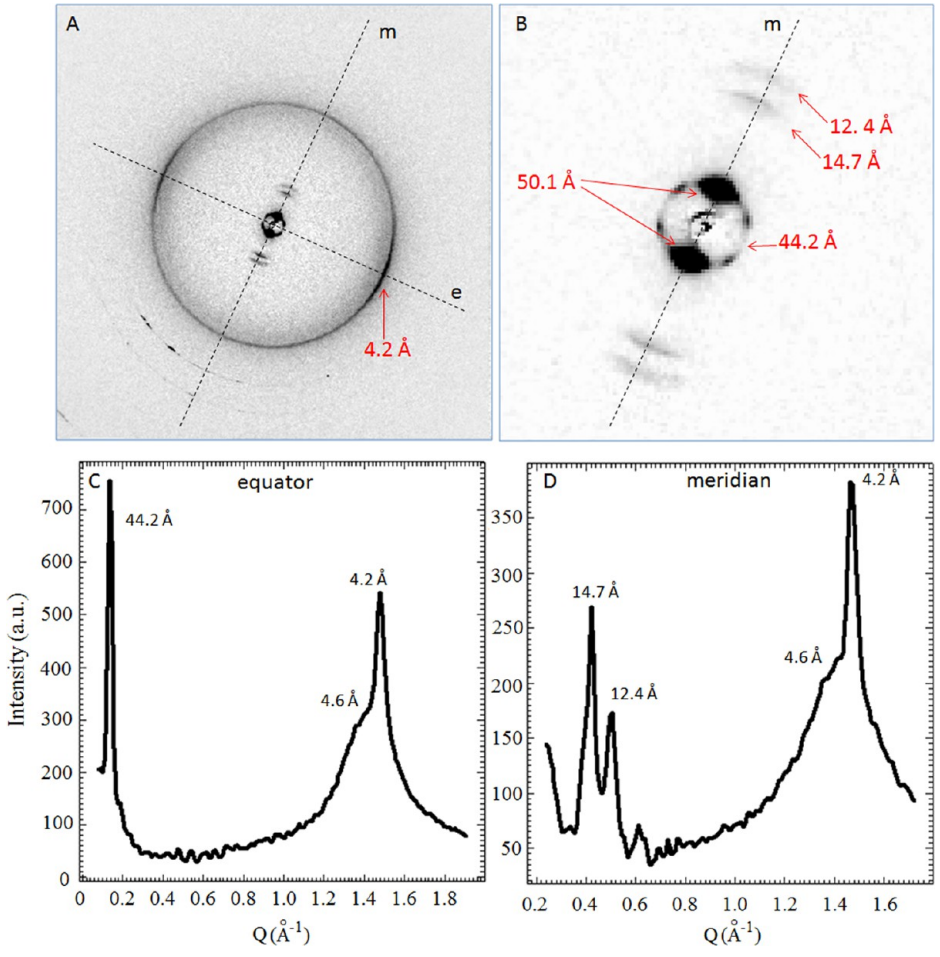

Figure 6. (A) Typical oriented pattern of the pure lipids residue. (B) Close up of the peaks at low angles of the XRD pattern in part A. (C) Azimuthal average of a typical pattern (A) in the equatorial region. (D) Azimuthal average of a typical pattern (A) in the meridional region. ($Q = 4\pi \sin \Theta/\lambda$, where λ is the X-ray wavelength and Θ the diffraction angle).

the 4.6 Å ring to a randomly oriented liquid phase and the 4.2 Å peak to the acyl chains of a gel phase.[32,33] The 44.2 Å powder ring is attributed to the lamellar stacking period of the gel-phase.

Further narrow reflections on the meridian (Figure 6B) are attributed to higher orders of lamellar periods of two highly ordered phospholipid phases. The strong meridional reflection is a composite peak including both a 50.1 Å peak (order $n = 1$ for the 12.4 Å reflection) and a 44.2 Å one (order $n = 1$ for the 14.7 Å reflection).[34] The four off-meridian reflections at $d =$ 44.2 Å are tentatively attributed to satellites of the $n = 1$ order of a ripple phase.

dx.doi.org/10.1021/la500145r | *Langmuir* 2014, 30, 3191−3198

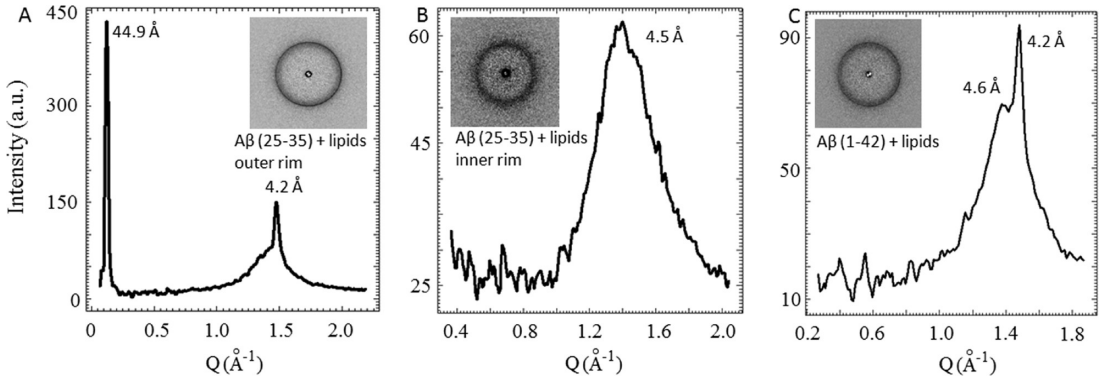

Figure 7. Azimuthal averages and relative diffraction patterns of POPC/POPS system mixed with Aβ peptides.

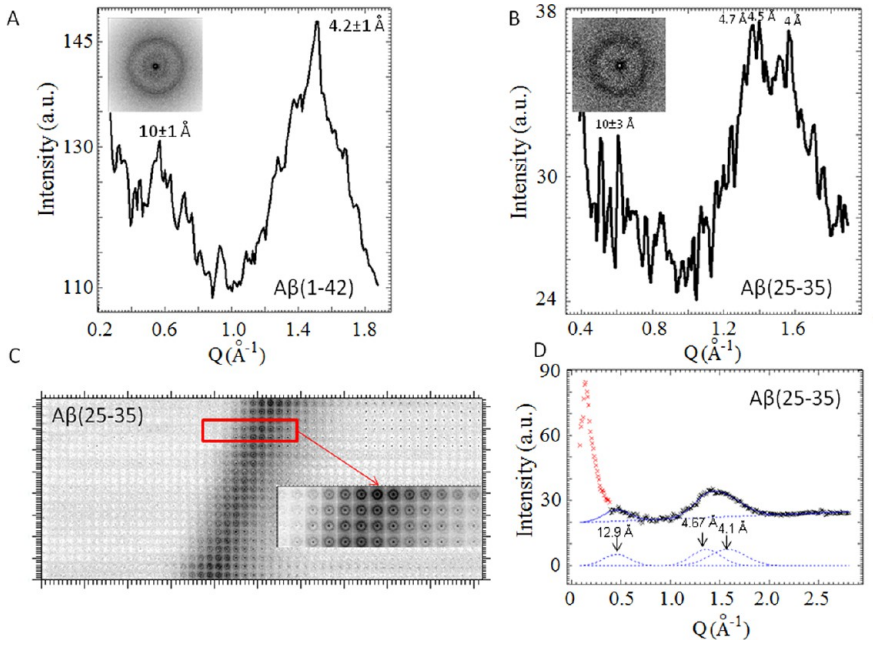

Figure 8. Typical μXRD mesh scan and relative azimuthal averages of the Aβ(1−42) (A) and Aβ(25−35) (B) droplet rims. (C) Mesh-scan of the Aβ(25−35) solid rim. (D) Peak fitting of the Aβ(25−35) XRD pattern of part B (three Gaussians and a first-order polynomial background were used. The red part of the plot was masked for the peak fitting).

The highly oriented structure is disrupted when Aβ protein is added, as shown also in previous studies.[35] Indeed, a mesh-scan of the rim of Aβ + POPC/POPS residues reveals only powder rings. This is shown for selected diffraction patterns in Figure 7. A ∼44.9 Å powder ring remains for the Aβ (25−35) + POPC/POPS in the outer and inner rim [Figures 7A,B and S5 (Supporting Information)] and a less intense one for the Aβ(1−42) + POPC/POPS residue [Figures 7C and S6 (Supporting Information)]. The double WAXS peak at 4.6 and 4.2 Å is visible in the outer rim of the Aβ(25−35) + POPC/POPS residual (Figure 7A) and in the Aβ(1−42) + POPC/POPS one (Figure 7C). The detection of β-type material was difficult for Aβ(25−35) + POPC/POPS and Aβ(1−42) + POPC/POPS, as the WAXS peaks of the lipids were essentially overlapping in the region of the hydrogen-bonded strands characteristic of β-sheet materials[16,17,36] (∼4.5 Å spacing). After a proper background subtraction (an average of several patterns taken from the same region was performed to increase the statistic and the same amount of background patterns were averaged prior to subtraction), we detected an isotropic broad peak centered at 4.5 Å in the inner rim of the Aβ(25−35) + POPC/POPS solution (Figure 7B). Due to the overlapping of the above-mentioned reflections, it was not possible to assign in an unambiguous way this component to the lipid liquid phase (4.6 Å) or to a short-range ordered β-sheet material. Further, the absence of the ∼10 Å diffraction peak probably indicates a disorder in the stacking of the protein intersheets.[37] Finally, it is clear how the lipid gel-phase (represented by the 4.2 Å peak) was concentrated in the outer rim of the Aβ(25−35) + POPC/POPS residual (Figure 7A) while in the inner one we could detect just the SAXS peak at ∼44.2 Å (Figure S5, Supporting Information). In both tested solutions [Aβ(1−42) + POPC/POPS and Aβ(25−35) + POPC/POPS] anyway it was not possible to detect the high orientation found for the pure phospholipid droplets (Figure 6), suggesting a severe disordering effect on the lamellar order of the lipid bilayer caused by the administration of the Aβ protein.[35]

Finally, in Figure 8, we show typical μXRD mesh scans and relative azimuthal averages of the pure Aβ(25−35) and Aβ(1−42) droplet solid rims. The pure Aβ(1−42) pattern shows β-sheet features with a 4.2 Å peak characteristic of the distance

dx.doi.org/10.1021/la500145r | Langmuir 2014, 30, 3191−3198

between hydrogen-bonded strands and a 10 Å peak due to the β-sheet stacking[38] (Figure 8A). A slight orientation, in terms of meridional and equatorial axes, can be seen in Figure S7 (Supporting Information). In contrast, the Aβ(25−35) rim shows only a very weak signature of a peak in the range of 10 Å, suggesting stacking disorder (Figure 8B). The rather large width of the peak of about $4.8 > d$ (Å) > 4, mainly due to the low amount of deposited material, suggests the copresence of β-sheet and α-helical material.[36] A more detailed analysis of the peak profile by fitting Gaussian functions shows a slight shoulder with $d \sim 12.9$ Å linked to the potential presence of a component in the region of the β-sheet stacking, but which cannot be concluded in a definitive way. On the other hand, a composite peak with $d \sim 4.7/4.1$ Å (Figure 8D) agrees with the possible coexistence of a β-phase (4.1 Å) together with a α-phase[36] (∼4.7 Å). For the latter one, a final quantitative separation was not possible, as the expected 5.5 Å peak of the α-helical period could not be clearly resolved by the peak fitting.

This follows in some way the results obtained by the μFTIR experiments, where the absence of the phospholipid system induced the clear presence of both β-sheet and α-helical material. The X-ray diffraction peak assignment in the range 4.1−4.7 Å, both for lipids and Aβ, is shown in Table 1.

Table 1. X-ray Diffraction Peak Assignment for the Aβ and Lipids Samples in the Range 4.1−4.7 Å

	Aβ	lipids
4.1/4.2 Å[18,38]	β-sheet	
4.2 Å[32,33]		acyl chains of ordered gel phase
4.5 Å[36]	β-sheet	
4.6 Å[32,33]		random oriented liquid phase
4.7 Å[36]	α-helix	

CONCLUSIONS

In this work, we studied conformational changes of Aβ(25−35) peptide in the presence and absence of a phospholipid system, namely POPC/POPS, by μRaman, SR μFTIR, and μXRD. Coffee-ring residues were obtained from the evaporation of pure and mixed solutions of Aβ(25−35) and POPC/POPS on highly hydrophilic substrates. Preliminary μRaman analysis showed the prominent presence of β-sheet material and, possibly, traces of α-helical material in Aβ(25−35) residues. As the overlapping of the POPC/POPS and peptide μRaman signatures did not allow confirming this, SR μFTIR experiments were performed. The results showed the presence of an α/β transition from the internal rim of the coffee-ring residues to the external one in the pure Aβ(25−35) residue, probably due to the convective flow inside the droplet sitting on highly hydrophilic substrates that enhances the local concentration of the protein at the external edge of the drying drop. In contrast, the presence of POPC/POPS lipids in the protein did not result in α-helical structures and introduced the presence of antiparallel β-sheet material together with parallel β-sheet structures and possible β-turns. This confirms how the presence of phospholipids seems to influence the fibrillation process, as hypothesized in previous studies.[29,30] As control we tested also the Aβ(1−42) peptide, which always showed β-sheet conformations independently from the presence of the lipid system. Further μXRD analysis of the same residues showed the presence of highly ordered lamellar structures in the phospholipid vesicle system. The administration of the Aβ protein provoked on the other hand a severe disorder in this arrangement, but as our attention in the present work was more focused on the α-helical/β-sheet conformations rather on the disruption mechanism of lipids, this process will be further examined. From another perspective, the absence of the phospholipid system induced in the Aβ(25−35) a probable composite α/β material, confirming the μFTIR experiments while its coexistence with the protein resulted in a not oriented β-sheet conformation. Further work on the subject could help clarify the role of enzymes such as acetylcholinesterase[39,40] and alternative lipid systems in the amyloidosis of the analyzed peptides and of other Aβ fragments.

ASSOCIATED CONTENT

Supporting Information

Further details about the μFTIR and μXRD experiments. This material is available free of charge via the Internet at http://pubs.acs.org.

AUTHOR INFORMATION

Corresponding Authors

*A.A.: tel, +3901071781847; fax, +3901071781236; e-mail, angelo.accardo@iit.it.

*S.D.: tel, +3901071781541; fax, +3901071781236; e-mail, silvia.dante@iit.it.

Author Contributions

The manuscript was written through contributions of all authors. All authors have given approval to the final version of the manuscript.

Notes

The authors declare no competing financial interest.

ABBREVIATIONS USED

Aβ, amyloid beta; APP, amyloid precursor protein; SR, synchrotron radiation; μXRD, micro X-ray diffraction; POPC, 1-palmitoyl-2-oleoylphospatidylcholine; POPS, 1-palmitoyl-2-oleoylphospatidylserine; SEM, scanning electron microscopy; μSAXS/WAXS, micro small and wide angle X-ray scattering; FTIR, Fourier-transform infrared spectroscopy.

REFERENCES

(1) Colletier, J. P.; Laganowsky, A.; Landau, M.; Zhao, M.; Soriaga, A. B.; Goldschmidt, L.; Flot, D.; Cascio, D.; Sawaya, M. R.; Eisenberg, D. Molecular Basis for Amyloid-Beta Polymorphism. *Proc. Natl. Acad. Sci. U. S. A.* **2011**, *108*, 16938−16943.

(2) Rocha, S.; Loureiro, J. A.; Brezesinski, G.; Pereira Mdo, C. Peptide−Surfactant Interactions: Consequences for the Amyloid-Beta Structure. *Biochem. Biophys. Res. Commun.* **2012**, *420*, 136−140.

(3) Williams, T. L.; Louise, C. S. Membrane and Surface Interactions of Alzheimer's Aβ Peptide—Insights into the Mechanism of Cytotoxicity. *FEBS J.* **2011**, *278*, 3905−3917.

(4) Mucke, L.; Selkoe, D. J. Neurotoxicity of Amyloid β-Protein: Aynaptic and Network Dysfunction. *Cold Spring Harbor Perspect. Med.* **2012**, *2*, a006338.

(5) Butterfield, S. M.; Lashuel, H. A. Amyloidogenic Protein−Membrane Interactions: Mechanistic Insight from Model Systems. *Angew. Chem., Int. Ed.* **2010**, *49*, 5628−5654.

(6) Burke, K. A.; Yates, E. A.; Legleiter, J. Biophysical Insights into how Surfaces, Including Lipid Membranes, Modulate Protein Aggregation Related to Neurodegeneration. *Front. Neurol.* **2013**, *4*, 1−17.

(7) Terzi, E.; Hölzemann, G.; Seelig, J. Interaction of Alzheimer β-Amyloid Peptide(1−40) with Lipid Membranes. *Biochemistry* **1997**, *36*, 14845−14852.
(8) Yip, C.; Mc Laurin, J. Amyloid-Beta Peptide Assembly: A Critical Step in Fibrillogenesis and Membrane Disruption. *Biophys. J.* **2001**, *80*, 1359−1371.
(9) Demuro, A.; Mina, E.; Kayed, R.; Milton, S. C.; Parker, I.; Glabe, C. G. Calcium Dysregulation and Membrane Disruption as a Ubiquitous Neurotoxic Mechanism of Soluble Amyloid Oligomers. *J. Biol. Chem.* **2005**, *280*, 17294−17300.
(10) Dante, S.; Hauss, T.; Steitz, R.; Canale, C.; Dencher, N. A. Nanoscale Structural and Mechanical Effects of β-Amyloid (1−42) on Polymer Cushioned Membranes: A Combined Study by Neutron Reflectometry and AFM Force Spectroscopy. *Biochim. Biophys. Acta* **2011**, *1808*, 2646−2655.
(11) Butterfield, D. A. Amyloid β-peptide (1−42)-induced Oxidative Stress and Neurotoxicity: Implications for Neurodegeneration in Alzheimer's Disease Brain. A Review. *Free Radical Res.* **2002**, *36*, 1307−1312.
(12) Dante, S.; Hauss, T.; Brandt, A.; Dencher, N. A. Membrane Fusogenic Activity of the Alzheimer's Peptide Aβ(1−42) Demonstrated by Small-Angle Neutron Scattering. *J. Mol. Biol.* **2008**, *376*, 393−404.
(13) Buchsteiner, A.; Hauss, T.; Dante, S.; Dencher, N. A. Alzheimer's Desease Amyloid β Peptide Analogue Alters the Picosecond Dynamics of Phospholipid Membranes. *Biochim. Biophys. Acta* **2010**, *1798*, 1969−1976.
(14) Mattson, M. P.; Cheng, B.; Davis, D.; Bryant, K.; Lieberburg, I.; Rydel, R. E. Amyloid Peptides Destabilize Calcium Homeostasis and Render Human Cortical Neurons Vulnerable to Excitotoxicity. *J. Neurosci.* **1992**, *12*, 376−389.
(15) Accardo, A.; Burghammer, M.; Di Cola, E.; Reynolds, M.; Di Fabrizio, E.; Riekel, C. Calcium Carbonate Mineralization: X-ray Microdiffraction Probing of the Interface of an Evaporating Drop on a Superhydrophobic Surface. *Langmuir* **2011**, *27*, 8216−8222.
(16) Accardo, A.; Mecarini, F.; Leoncini, M.; Brandi, F.; Di Cola, E.; Burghammer, M.; Riekel, C.; Di Fabrizio, E. Fast, Active Droplet Interaction: Coalescence and Reactive Mixing Controlled by Electrowetting on a Superhydrophobic Surface. *Lab Chip* **2013**, *13*, 332−335.
(17) Hauser, C. A. E.; Mishra, A.; Deng, R.; Loo, Y.; Zhuang, F.; Khoe, U.; Cheong, D. W.; Accardo, A.; Sullivan, M. B.; Riekel, C.; Ying, J.; Hauser, U. Natural Tri- to Hexapeptides Self-Assemble in Water to Amyolid β-type Fiber Aggregates by Unexpected α-Helical Intermediate Structures. *Proc. Natl. Acad. Sci. U. S. A.* **2011**, *108*, 1361−1366.
(18) Accardo, A.; Burghammer, M.; Di Cola, E.; Reynolds, M.; Di Fabrizio, E.; Riekel, C. Lysozyme Fibrillation Induced by Convective Flows Under Quasi Contact-Free Conditions. *Soft Matter* **2011**, *7*, 6792−6796.
(19) Accardo, A.; Tirinato, L.; Altamura, D.; Sibillano, T.; Giannini, C.; Riekel, C.; Di Fabrizio, E. Superhydrophobic Surfaces Allow Probing of Exosome Self Organization Using X-ray Scattering. *Nanoscale* **2013**, *5*, 2295−2299.
(20) Vaughan, G. B. M.; Wright, J. P.; Bytchkov, A.; Rossat, M.; Gleyzolle, H.; Snigireva, I.; Snigirev, A. X-ray Transfocators: Focusing Devices Based on Compound Refractive Lenses. *J. Synchrotron Radiat.* **2011**, *18*, 125−133.
(21) Blanton, T. N.; Huang, T. C.; Toraya, H.; Hubbard, C. R.; Robie, S. B.; Louër, D.; Göbel, H. E.; Will, G.; Gilles, R.; Raftery, T. JCPDS-International Centre for Diffraction Data Round Robin Study of Silver Behenate. A Possible Low-Angle X-ray Diffraction Calibration Standard. *Powder Diffr.* **1995**, *10*, 91−95.
(22) Tuma, R.; Bamford, J. H. K.; Bamford, D. H.; Thomas, G. J. Structure, Interactions and Dynamics of PRD1Virus II. Organization of the Viral Membrane and DNA. *J. Mol. Biol.* **1996**, *257*, 102−115.
(23) Maiti, N. C.; Apetri, M. M.; Zagorski, M. G.; Carey, P. R.; Anderson, V. E. Raman Spectroscopic Characterization of Secondary Structure in Natively Unfolded Proteins: α-Synuclein. *J. Am. Chem. Soc.* **2004**, *126*, 2399−2408.
(24) Wang, Y.; Purrello, R.; Jordan, T.; Spiro, T. G. UVRR Spectroscopy of the Peptide Bond. 1. Amide S, a Nonhelical Structure Marker, is a C.alpha.H Bending Mode. *J. Am. Chem. Soc.* **1991**, *113*, 6359−6368.
(25) Lee, C.; Bain, C. D. Raman Spectra of Planar Supported Lipid Bilayers. *Biochim. Biophys. Acta* **2005**, *1711*, 59−71.
(26) Naumann, D. Infrared Spectroscopy in Microbiology. In *Encyclopedia of Analytical Chemistry*; Meyers, R. A., Ed.; John Wiley & Sons Ltd.: New York, 2000.
(27) Deegan, R. D.; Bakajin, O.; Dupont, T. F.; Huber, G.; Nagel, S. R.; Witten, T. A. Capillary Flow as the Cause of Ring Stains from Dried Liquid Drops. *Nature* **1997**, *389*, 827−829.
(28) Hu, H.; Larson, R. G. Analysis of the Microfluid Flow in an Evaporating Sessile Droplet. *Langmuir* **2005**, *21*, 3963−3971.
(29) Sheikh, A. M.; Nagai, A. Lysophosphatidylcholine Modulates Fibril Formation of Amyloid β Peptide. *FEBS J.* **2011**, *278*, 634−642.
(30) Martins, I. C.; Kuperstein, I.; Wilkinson, H.; Maes, E.; Vanbrabant, M.; Jonckheere, W.; Van Gelder, P.; Hartmann, D.; D'Hooge, R.; De Strooper, B.; Schymkowitz, J.; Rousseau, F. Lipids Revert Inert Aβ Amyloid Fibrils to Neurotoxic Protofibrils that Affect Learning in Mice. *EMBO J.* **2008**, *27*, 224−233.
(31) Sarroukh, R.; Goormaghtigh, E.; Ruysschaert, J. M.; Raussens, V. ATR-FTIR: A "Rejuvenated" Tool To Investigate Amyloid Proteins. *Biochim. Biophys. Acta* **2013**, *1828*, 2328−38.
(32) Cunningham, B. A.; Brown, A. D.; Wolfe, D. H.; Williams, W. P.; Brain, A. Ripple Phase Formation in Phosphatidylcholine: Effect of Acyl Chain Relative Length, Position, and Unsaturation. *Phys. Rev. E* **1998**, *58*, 3662−3672.
(33) Mills, T. T.; Huang, J.; Feigenson, G. W.; Nagle, J. F. Effects of Cholesterol and Unsaturated DOPC Lipid on Chain Packing of Saturated Gel-Phase DPPC Bilayers. *Gen. Physiol. Biophys.* **2009**, *28*, 126−139.
(34) Hristova, K.; White, S. H. Determination of the Hydrocarbon Core Structure of Fluid Dioleoylphosphocholine (DOPC) Bilayers by X-ray Diffraction Using Specific Bromination of the Double-Bonds: Effect of Hydration. *Biophys. J.* **1998**, *74*, 2419−33.
(35) Dante, S.; Hauss, T.; Dencher, R. A. Insertion of Externally Administered Amyloid β Peptide 25−35 and Perturbation of Lipid Bilayers. *Biochemistry* **2003**, *42*, 13667−13672.
(36) Drummy, L. F.; Phillips, D. M.; Stone, M. O.; Farmer, B. L.; Naik, R. R. Thermally Induced α-Helix to β-sheet Transition in Regenerated Silk Fibers and Films. *Biomacromolecules* **2005**, *6*, 3328−3333.
(37) Wang, K.; Keasling, J. D.; Muller, S. J. Effects of the Sequence and Size of Non-Polar Residues on Self-Assembly of Amphiphilic Peptides. *Int. J. Biol. Macromol.* **2005**, *36*, 232−240.
(38) Marsh, R. E.; Corey, R. B.; Pauling, L. An Investigation of the Structure of Silk Fibroin. *Biochim. Biophys. Acta* **1955**, *16*, 1−34.
(39) Inestrosa, N. C.; Alvarez, A.; Pérez, C. A.; Moreno, R. D.; Vicente, M.; Linker, C.; Casanueva, O. I.; Soto, C.; Garrido, J. Acetylcholinesterase Accelerates Assembly of Amyloid-Beta-Peptides into Alzheimer's Fibrils: Possible Role of the Peripheral Site of the Enzyme. *Neuron* **1996**, *16*, 881−91.
(40) Dinamarca, M. C.; Sagal, J. P.; Quintanilla, R. A.; Godoy, J. A.; Arrázola, M. S.; Inestrosa, N. C. Amyloid-β-Acetylcholinesterase Complexes Potentiate Neurodegenerative Changes Induced by the Aβ Peptide. Implications for the Pathogenesis of Alzheimer's Disease. *Mol. Neurodegener.* **2010**, *5*, 1−15.